Dirac scattered-wave calculations on an icosahedral Au_{13} cluster

Agustin F. Ramos, Ramiro Arratia-Perez,* and Gulzari L. Malli
Department of Chemistry and Theoretical Sciences Institute, Simon Fraser University, Burnaby, British Columbia, Canada V5A 1S6

(Received 22 August 1986; revised manuscript received 6 November 1986)

Symmetry-adapted angular-momentum basis functions have been generated for the icosahedral double point group (I_h^*). These basis functions are used to obtain the relativistic molecular orbitals for the icosahedral Au_{13} cluster via the self-consistent-field Dirac scattered-wave method. Nonrelativistic-limit calculations are also reported for the ground state of the Au_{13} cluster in order to ascertain the importance of relativistic effects in such heavy-atom systems. The ionization potential and the lowest dipole-allowed electronic transitions are predicted using the spin-restricted transition state formalism. The calculated density of states for the Au_{13} cluster shows similar features to those obtained in photoemission experiments of small clusters of gold on various substrates. Relativistic effects increase the d-bandwidth of Au_{13} to 3.9 eV, and spin-orbit interactions split the d band into the $d_{3/2}$ and $d_{5/2}$ subbands by 2.2 eV. These calculated results are in very good agreement with the values obtained from the x-ray photoemission spectra of the valence band of gold clusters. Due to relativity, an increased overlap of the s and d bands is observed, leading to appreciable s-d hybridization in the cluster-bonding molecular orbitals.

I. INTRODUCTION

The recent discovery[1] of an ordered structure characterized by a fivefold symmetry axis (which is incompatible with translational symmetry) in Al-Mn alloys has attracted considerable attention.[2–4] The x-ray diffraction and electron diffraction patterns of these alloys indicate the existence of a material which exhibits long-range icosahedral rotational symmetry.[1–4] Icosahedral quasicrystals of Al-Cu-Li formed by solid-state reaction have also been recently confirmed by convergent-beam electron diffraction (CBED) patterns.[5] Thus there exists overwhelming experimental data in favor of a novel class of icosahedral ordered structures in the solid state.[1–5] However, the icosahedral geometry is quite well known at the molecular level, e.g., it occurs in elemental boron and its compounds[6] which were treated theoretically thirty years ago by Longuet-Higgins and Roberts.[7] A number of transmission electron microscopy (TEM) studies have indicated that icosahedral gold particles were formed at the earliest stage of gold film growth on alkali-halide crystals.[8–11] Recently, the ESR spectral data[12] have suggested an icosahedral arrangement for Sc_{13}, while a few years ago the successful synthesis of an icosahedral gold-phosphine cluster $[Au_{13}L_{10}Cl_2]^{3+}$ was announced,[13] where L is a triarylphosphine ligand.

A variety of nonrelativistic methods have been used in order to elucidate the electronic structure of icosahedral metallic clusters; viz., the Hückel molecular-orbital (HMO) method for the Au_{13}^{5+} cluster,[14] the self-consistent-field scattered-wave (SCF-SW) method for the Sc_{13} cluster,[15] Al_{13} cluster, and $Al_{12}Mn$ alloy,[16] and *ab initio* SCF linear combination of atomic orbitals (LCAO's) method for the Cu_{13} cluster.[17] This is no doubt, in part, due to the fact that the electronic structure and physical properties of small metallic clusters are a subject of extensive theoretical and experimental research at present, because of their relevance to surface phenomena, growth morphology, and heterogeneous catalysis.[18–20] In this context the icosahedral Au_{13} cluster can serve as a model for heavy metal clusters and microcrystallites, and the elucidation of its electronic structure and optical properties could be useful for the research in the field of catalysis and surface phenomena.

Although an *ab initio* all-electron nonrelativistic calculation has been reported for the icosahedral Cu_{13} cluster,[17] a similar nonrelativistic calculation on Au_{13} is currently unfeasible. Moreover, it has been shown by fully *ab initio* Dirac-Fock calculation on AuH,[21] and by Dirac scattered-wave (DSW) calculations on Au_n^{q+} ($n=3$, 4, and 6; $q=1$ and 2) clusters,[22–23] that the nonrelativistic description of chemical bonding for these heavy-atom systems is unrealistic, since there is significant "s-d" hybridization in the bonding molecular orbitals, due to relativistic effects. Since fully *ab initio* all-electron Dirac-Fock calculations for systems as large as Au_{13} are unthinkable at present, we report here for the first time a fully relativistic SCF-DSW calculation for an icosahedral Au_{13} cluster, in order to investigate the importance of relativistic effects in chemical bonding, optical spectra, density of states (DOS), and first ionization potential of this heavy metal cluster.

II. METHOD OF CALCULATION

A. DSW Method

The SCF Dirac scattered-wave (DSW) molecular-orbital method is the relativistic extension (in the full four-component Dirac formalism) of the nonrelativistic multiple scattering or scattered-wave technique developed by Johnson.[24] The DSW methodology was developed by Yang and co-workers,[25–28] and except for the change of

boundary conditions it is analogous to the relativistic Korringa-Kohn-Rostoker (RKKR) technique for solids.[29] It is now well established that relativistic effects are important in understanding the electronic structure, optical, and magnetic properties of systems, involving heavy transition metals,[30–34] lanthanides, and actinides.[35,36] The DSW formalism uses the Dirac equation rather than the Schrödinger equation to generate the one-electron orbitals, and thus implicitly includes all the so-called relativistic effects such as spin-orbit interaction, Darwin, and mass-velocity corrections. Basically, the DSW method incorporates two fundamental assumptions: first, that the wave function can be approximated as a Slater determinant of four-component molecular spinors determined by an effective Coulomb and exchange-correlation potential; and secondly, that this potential is spherically averaged inside cells surrounding each atomic nucleus, and outside an outer sphere that surrounds the entire molecule or cluster. The orbital energies are determined by solving the DSW secular equations and the resulting molecular spinors transform according to the extra irreducible representations (irreps) of the molecular double point group under study.

The parameters used for the calculations (assuming overlapping spheres) reported here are given in Table I, and the coordinate system for the icosahedral geometry of the Au_{13} cluster is shown in Fig. 1. A minimum basis of angular functions was used, with $l \leqq 4$ on the outer sphere and $l \leqq 2$ on the metal. The basis functions for the I_h^* double point group were generated according to the symmetrization procedure of Yang[37] and are discussed in the following section. The nonrelativistic-limit calculations were obtained by using a large value of $c = 10^{15}$ a.u. in order to estimate quantitatively the relativistic effects. Each iteration of the SCF calculation required about 45 sec on a Cray-1 computer and about 40 iterations were required to achieve convergence.

B. Symmetry-adapted basis functions

The icosahedral point group I_h has ten single-valued irreducible representations (irreps) and eight double-valued or extra irreps. Omitting for simplicity the g or u (subscript of parity) designation of the irreps, the single-valued irreps of dimensions 1, 3, 3, 4, and 5 are denoted by A, T_1, T_2, G, and H, respectively, while the extra irreps of dimensions 2, 2, 4, and 6 are denoted by E_2, E_3, Q, and I. The descent in symmetry from the full rotation group to the icosahedral double group I_h^* is shown in Table II. It can be seen from Table II that the atomic levels at the center of symmetry with orbital angular momentum $l \leqq 2$ are not split by the icosahedral crystal field; however, the degeneracy of levels with $l \geqq 3$ is removed, in contrast to the symmetry group of the sphere in which the degeneracy of the atomic levels is not lifted. A simple reduction of the direct products of the single-valued irreps (omitting g and u character) with the two-dimensional spin representation E_{2g} in terms of the double-valued irreps of I_h^* gives all the compatibility relations between them, namely,

$$A \times E_{2g} \rightarrow E_2 ,$$
$$T_1 \times E_{2g} \rightarrow E_2 + Q ,$$
$$T_2 \times E_{2g} \rightarrow I ,$$
$$G \times E_{2g} \rightarrow E_3 + I ,$$
$$H \times E_{2g} \rightarrow Q + I .$$

This shows that $p(T_{1u})$ and $d(H_g)$ subshells of an atom

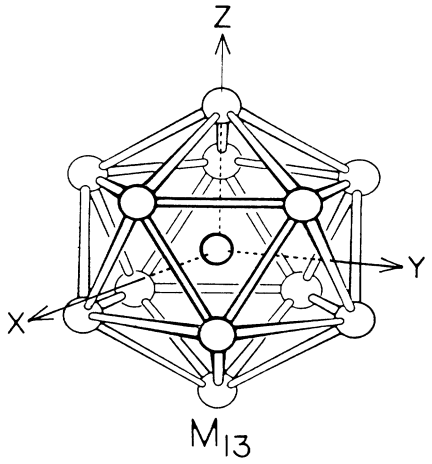

FIG. 1. The icosahedral Au_{13} cluster.

TABLE I. Parameters used in the calculations. Au(1) denotes the central atom and Au(2) denotes a peripheral atom. Interatomic distances were taken from the crystallographic data of the icosahedral $[Au_{13}L_{10}Cl_2]^{3+}$ cluster (see Ref. 13).

	Au_{13}
Au(1)—Au(2) distance (Å)	2.75
Au(2)—Au(2′) distance (Å)	2.89
Point group symmetry	I_h
Exchange-correlation (α)	0.693 01
Au(1) sphere radius (Å)	1.33
Au(2) sphere radius (Å)	1.49
Outer sphere radius (Å)	4.14

TABLE II. Full rotation group compatibility table for the I_h^* group. Descent in symmetry from the full rotation group irreps $D_j^{\pm}$ ($j = 0, 1/2, 1, \ldots, \frac{7}{2}$) to the I_h^* group irreps.

$D_0^+(s_0)$[a]	A_g	D_0^-	A_u
$D_{1/2}^+(s_{1/2})$	E_{2g}	$D_{1/2}^-(p_{1/2})$	E_{2u}
D_1^+	T_{1g}	$D_1^-(p_1)$	T_{1u}
$D_{3/2}^+(d_{3/2})$	Q_g	$D_{3/2}^-(p_{3/2})$	Q_u
$D_2^+(d_2)$	H_g	D_2^-	H_u
$D_{5/2}^+(d_{5/2})$	I_g	$D_{5/2}^-(f_{5/2})$	I_u
D_3^+	$T_{2g}+G_g$	$D_3^-(f_3)$	$T_{2u}+G_u$
$D_{7/2}^+(g_{7/2})$	$E_{3g}+I_g$	$D_{7/2}^-(f_{7/2})$	$E_{3u}+I_u$

[a]Subshell type l_j for angular-momentum functions at the central site.

TABLE III. Symmetrized basis functions of I_h^* group for Au_{13}.

l	κ[a]	j	Central atom	Twelve peripheral atoms
0	-1	$\frac{1}{2}$	e_{2g}	$e_{2g}+e_{2u}+q_g+q_u+I_g+I_u$
1	1	$\frac{1}{2}$	e_{2u}	$e_{2g}+e_{2u}+q_g+q_u+I_g+I_u$
1	-2	$\frac{3}{2}$	q_u	$e_{2g}+e_{2u}+e_{3g}+e_{3u}+2q_g+2q_u+2I_g+2I_u$
2	2	$\frac{3}{2}$	q_g	$e_{2g}+e_{2u}+e_{3g}+e_{3u}+2q_g+2q_u+2I_g+2I_u$
2	-3	$\frac{5}{2}$	I_g	$e_{2g}+e_{2u}+e_{3g}+e_{3u}+2q_g+2q_u+4I_g+4I_u$

[a]The κ quantum number defines both l and j through $\kappa=-(j+\frac{1}{2})a$; $a=1$ for $j=l+\frac{1}{2}$ and $a=-1$ for $j=l-\frac{1}{2}$.

placed at the center of symmetry are split by spin-orbit interaction into $p_{1/2}(e_{2u})$ plus $p_{3/2}(q_u)$, and $d_{3/2}(q_g)$ plus $d_{5/2}(I_g)$, respectively. It should be mentioned that multicenter symmetrized functions for the icosahedral double group have not been reported in the literature, and so we constructed the multicenter (i.e., involving 12 peripheral atoms) symmetry-adapted basis functions for I_h^* using Yang's[37] procedure, by projecting the atomic spinors onto the basis set of each extra irrep of I_h^*. By inspection of the compatibility relations given in Table II, the representation matrices required for the construction of the projection operators were chosen as the rotation matrices[38] D_j ($j=\frac{1}{2}$, $\frac{3}{2}$, and $\frac{5}{2}$) for e_2, q, and I, respectively. For e_3, a representation was generated by block diagonalizing the matrices for $D_{7/2}$ since $D_{7/2}\rightarrow e_3+I$. This block diagonalization was achieved by means of the projection operator P^i defined[39] by

$$P^i=l_i/g\sum_R \chi^{i*}(R)D_j(R)\ , \tag{1}$$

where g is the order of the group and $\chi^i(R)$ is the character of the representation matrix for the rotation R in the ith irrep of dimension l_i.

With $i=e_3$ and $j=\frac{7}{2}$, by applying the projector P^i onto the half-angular-momentum vectors $\{|j=\frac{7}{2},\mu\rangle\}$ spanning $D_{7/2}$, four nonzero vectors were projected and, according to the dimension of e_3, only two were linearly independent. After normalization, we choose

$$|e_3(1)\rangle=(\tfrac{7}{10})^{1/2}|\tfrac{7}{2},-\tfrac{3}{2}\rangle+(\tfrac{3}{10})^{1/2}|\tfrac{7}{2},\tfrac{7}{2}\rangle\ , \tag{2}$$

$$|e_3(2)\rangle=-(\tfrac{3}{10})^{1/2}|\tfrac{7}{2},-\tfrac{7}{2}\rangle+(\tfrac{7}{10})^{1/2}|\tfrac{7}{2},\tfrac{3}{2}\rangle \tag{3}$$

as the basis vectors spanning e_3. These vectors are the same as those reported by Raynal,[40] and from them the suitable transformation blocking $D_{7/2}$ into e_3 only[39] was built. Having obtained all the representation matrices, the symmetrized basis functions for the Au_{13} icosahedral cluster were simply generated by running the XJLM computer program[41] in a minimum atomic basis with truncation in angular momentum at $l=2$ for each Au atom. The breakdown of the symmetrized functions for the various extra irreps of I_h^* is given in Table III.

III. RESULTS AND DISCUSSION

A. Molecular orbitals

The nonrelativistic-limit and the relativistic (DSW) valence orbital energies are shown in Fig. 2. The

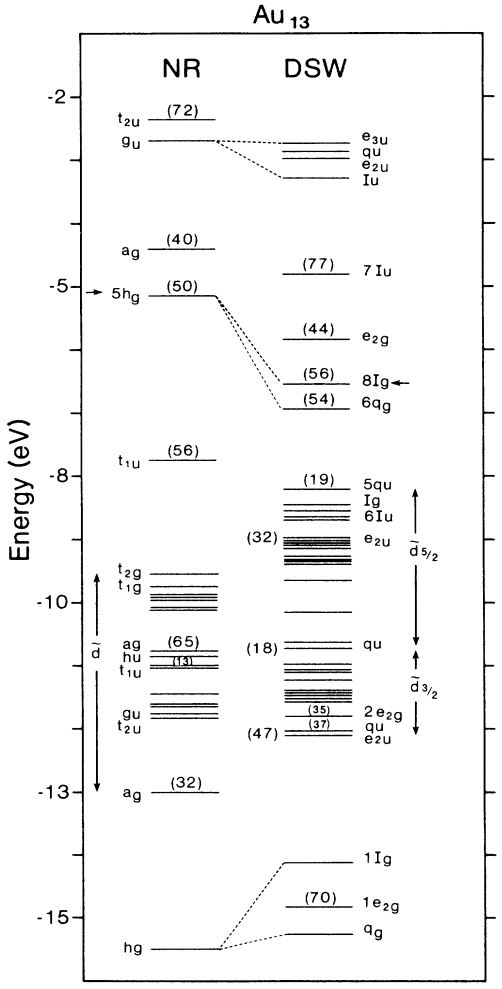

FIG. 2. Nonrelativistic (NR) limit and relativistic (DSW) valence energy levels and their corresponding symmetry. Numbers in parentheses give the percent 6s metal character, values less than 10% are not marked. The HOMO (or Fermi level) is indicated by an arrow in each case.

nonrelativistic-limit results show a valence structure which consists of an occupied d band and a partially filled s band associated mostly with the peripheral atoms, but below the d band is the h_g orbital which is mainly localized at the central atom. It is evident from Fig. 2 that the nonrelativistic results show that the s and d bands just begin to overlap at the top of the d band, where the lowest molecular orbital (MO) a_g consisting mainly of $6s$ (65%) atomic orbitals (AO's) is located. The analysis of the nonrelativistic wave function for Au_{13} indicates that most of the bonding molecular orbitals are located at the bottom of the d band, while most of the orbitals located near the top of the d band are either antibonding or nonbonding. Furthermore, the molecular orbitals with significant $6s$ contributions located in the d band (namely, a_g, t_{1u}, and a_g) are also bonding. The lowest occupied level h_g corresponds to a bonding MO between the central atom and the peripheral atoms involving mainly the $5d$ atomic orbitals. In addition, above the d band there are the antibonding orbitals t_{1u} and the highest occupied MO (HOMO) ($5h_g$) which are mainly $6s$-$6p$ hybrids. The lowest unoccupied MO (LUMO) (a_g) is also a $6s$-$6p$ hybrid and contains significant $6s$ (25%) contributions from the central atom. The remaining unoccupied MO's are either $6s$-$6p$ hybrids (t_{2u}) or almost pure nonbonding $6p$ atomic combinations (g_u). It is interesting to note that our nonrelativistic-limit results for Au_{13} resemble very closely the *ab initio* SCF-LCAO results[17] for the icosahedral Cu_{13} cluster. The or-

TABLE IV. Ground-state valence orbital populations (in terms of atomic spinors) (%).

		Au central atom					Au peripheral atoms				
Level	$-E$ (eV)	$s_{1/2}$	$p_{1/2}$	$p_{3/2}$	$d_{3/2}$	$d_{5/2}$	$s_{1/2}$	$p_{1/2}$	$p_{3/2}$	$d_{3/2}$	$d_{5/2}$
$3e_{3u}$	2.774								92.7	6.0	1.3
6_{qu}	2.861			16.6			2.4	41.2	35.0	1.2	3.6
$4e_{2u}$	2.980		25.9				1.2	12.2	49.8	0.0	10.9
$8I_u$	3.294						2.4	41.7	45.2	1.2	9.5
$7I_u$	4.810						76.8	10.9	5.5	2.7	4.1
$4e_{2g}$	5.844	26.3					18.0	9.3	18.6	4.6	23.2
$8I_g$	6.542[a]					3.3	56.4	1.2	23.6	1.2	14.3
$6q_g$	6.947				1.6		54.0	20.4	8.4	3.6	12.0
$5q_u$	8.220			1.7			19.2	0.0	7.2	2.4	69.5
$7I_g$	8.450					2.7	0.0	0.0	0.0	7.3	90.0
$6I_u$	8.554						0.0	2.4	1.2	0.0	96.4
$5q_g$	8.633				0.4		2.4	2.4	1.2	8.5	85.1
$6I_g$	8.708					1.2	1.2	0.0	2.4	10.8	84.8
$2e_{3u}$	8.990								1.2	17.9	80.9
$3e_{2u}$	9.002		0.4				32.4	9.4	2.4	24.7	30.7
$4q_g$	9.027				7.7		2.4	0.0	0.0	14.6	75.3
$4q_u$	9.033			1.7			0.0	2.4	0.0	15.8	80.1
$5I_u$	9.123						0.0	1.2	1.2	16.9	80.7
$3e_{2g}$	9.280	1.8					3.6	2.4	0.0	44.8	47.4
$4I_u$	9.312						2.4	1.2	0.0	21.7	74.7
$2e_{3g}$	9.350								0.0	20.2	79.8
$5I_g$	9.373					0.0	0.0	2.4	0.0	14.3	83.3
$3I_u$	9.666						0.0	0.0	1.2	13.3	85.5
$4I_g$	10.184					2.3	4.9	2.4	0.0	30.5	59.9
$3I_g$	10.632					16.0	3.6	0.0	0.0	37.2	43.2
$3q_u$	10.730			0.0			18.0	2.4	2.4	51.9	25.3
$2e_{2u}$	10.976		7.7				0.0	0.0	0.0	48.0	44.3
$3q_g$	11.086				0.5		0.0	0.0	0.0	94.7	4.8
$2q_u$	11.132			0.5			3.6	0.0	1.2	89.8	4.9
$1e_{3g}$	11.248								2.4	75.9	21.7
$2I_u$	11.407						0.0	1.2	1.2	73.5	24.1
$2I_g$	11.426					0.7	1.2	0.0	1.2	82.3	14.5
$2q_g$	11.468				2.0		7.2	0.0	2.4	76.5	11.9
$1e_{3u}$	11.520								3.6	77.4	19.0
$1I_u$	11.551						3.7	0.0	0.0	70.7	25.6
$2e_{2g}$	11.807	1.0					35.1	0.0	0.0	43.4	20.5
$1q_u$	12.033			6.8			37.2	3.7	3.7	36.5	12.1
$1e_{2u}$	12.106		6.3				46.8	0.0	9.4	24.6	12.9
$1I_g$	14.143					70.8	4.9	2.4	1.2	15.8	4.9
$1e_{2g}$	14.843	36.5					33.6	4.8	8.4	8.4	8.3
$1q_g$	15.244				85.6		3.6	0.0	2.4	0.0	8.4

[a]The HOMO is $8I_g$. Valence orbital population contributions forbidden by symmetry are not shown.

dering and the character of the energy levels are very much alike. In addition, both the *ab initio* SCF-LCAO (Ref. 17) (for Cu_{13}) and the present nonrelativistic-limit (for Au_{13}) calculations predict ^6A_g as the ground state arising from the electronic configuration (h_g^5) (i.e., the HOMO contains five unpaired electrons).

The relativistic (DSW) valence orbital energies are also shown in Fig. 2 for comparison. The most notable characteristic of the valence electronic structure of Au_{13} is the large splitting of the occupied d band into the $d_{3/2}$ and $d_{5/2}$ subbands due to spin-orbit interaction. The calculated d-band splitting of 2.2 eV is in excellent agreement with the values of 1.9 to 2.5 eV obtained from photoemission studies of small clusters of gold on various substrates.[42–45] The lowest occupied nonrelativistic-MO h_g, which is localized primarily on the central gold atom, is split by spin-orbit interaction into q_g and I_g MO's, and the calculated splitting is 1.1 eV (due to its $5d_{3/2}$ and $5d_{5/2}$ contents). That this splitting is somewhat smaller than 1.52 eV observed in Au atom[46] is a consequence of the strong bonding interactions between the central and the peripheral gold atoms. It can be seen from Fig. 2 that relativistic effects stabilize the MO's involving significant amounts of $6s$ atomic orbitals; however, the MO's with substantial $5d$ contributions are destabilized. Thus, due to relativity, significant "s-d" hybridization occurs in the valence MO's of this cluster. A comparison of the DSW and nonrelativistic total valence populations in the Au_{13} cluster reveals an increase of 2.1 electrons in the $6s$ populations, but a decrease of 1.9 electrons in the $5d$ populations.

The ground-state valence orbital populations obtained from the DSW calculation are given in Table IV. It can be seen that the central gold atom incorporated into the icosahedral site contributes only pure atomic spinors (i.e., not hybridized) to the extra irreps e_{2g}, e_{2u}, q_g, q_u, and I_g; however, it makes no contributions to the molecular orbitals which transform like the extra irreps e_{3g}, e_{3u}, and I_u, as dictated by double point group symmetry. Nevertheless, the peripheral atoms are *spd* hybridized (involving atomic spinors of any j value), except in the MO's that span the e_{3g} and e_{3u} extra irreps in which hybridization occurs only between $j=\frac{3}{2}$ and $j=\frac{5}{2}$ spinors. From Table IV it is clearly seen that the s band overlaps more effectively the d band due to relativistic effects. Most of the valence MO's are localized on the peripheral atoms and only the bonding $1q_g$ and $1I_g$ orbitals are primarily localized on the central atom. The bonding character of $1I_g$ can be seen from Fig. 3, where we present the contours of the large components of its wave function. The first Ψ_1 component, which is the dominant contribution to the $1I_g$ MO, shows the bonding interactions involving the $5d_{x^2-y^2}$ orbital of the central atom and the $6p_x$ and $6p_y$ orbitals of the upper pentagon of Au atoms. The second Ψ_2 component represents the spin-orbit contamination (β spin) to this MO and shows bonding interactions involving the $6p$ orbitals of the upper two Au atoms, and $6s$-$6p$ antibonding combinations between the Au atom along the x axis and its two nearest neighbors. The $5d$ participation in chemical bonding of the $1I_g$ MO can be seen from Fig. 4(a), while in Fig. 4(b) we present the contours of the dominant component of the $1e_{2g}$ MO and one can clearly see the symmetric bonding interactions between the central atom and the peripheral atoms, involving mainly the $6s$ atomic orbitals. Furthermore, there are strongly s-d hybridized bonding molecular orbitals $1e_{2u}$, $1q_u$, and $2e_{2g}$ (see Table IV), which are located at the bottom of the $d_{3/2}$ band, while in the $d_{5/2}$ band there are nonbonding and antibonding MO's involving mostly pure $5d$ combinations of the peripheral atoms.

Finally, the nonrelativistic HOMO ($5h_g$) (which contains five unpaired electrons giving rise to a ^6A_g ground state) splits by 0.4 eV due to spin-orbit interaction (because of its $6p_{1/2}$ and $6p_{3/2}$ contents) into the sixfold $8I_g$

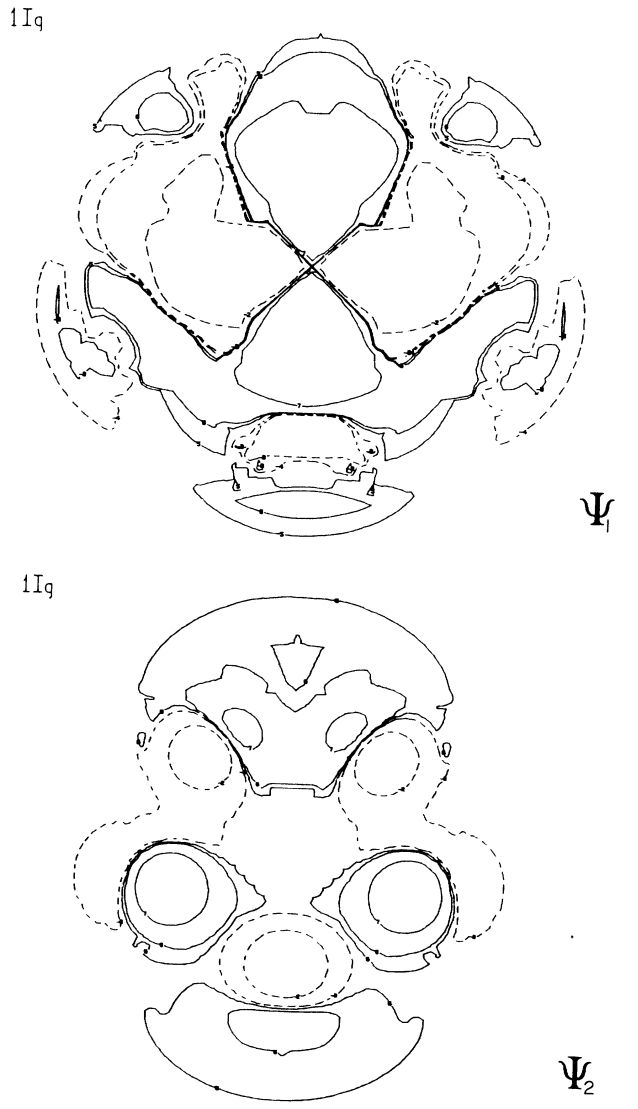

FIG. 3. Contours of the large components of $1I_g$ (XY plane) at $z=1.16$ a.u. Contour values in (electrons/bohr^3)$^{1/2}$ for the dominant component (Ψ_1) are between ±0.5 and ±0.005, while for Ψ_2 are between ±0.05 and ±0.0005, and are the same for all the contours presented here. Negative wave-function contours are given by dashed line.

and the fourfold $6q_g$ MO's. The calculated value of 0.4 eV for this splitting is in close agreement with the value of 0.47 eV reported for the $6p_{1/2}$-$6p_{3/2}$ splitting in the Au atom.[46] It is interesting to note that whereas the nonrelativistic-limit calculation predicts the sextet ^6A_g as the ground state for Au_{13} cluster, our DSW calculation predicts a doublet as the ground state ^2I_g due to relativistic effects (i.e., the single unpaired electron resides in the $8I_g$ molecular orbital). The immediate consequence of this result is that the relativistic formalism indicates that the Au_{13} cluster should show a weak paramagnetic susceptibility, in contrast to the nonrelativistic description which predicts a much stronger paramagnetic behavior. It would be interesting to verify these predictions for the icosahedral Au_{13} cluster when its magnetic susceptibility could be determined in future. The characteristics of the HOMO or Fermi level (E_F) $8I_g$ are shown in Fig. 5, and one can see in the dominant (α spin) component Ψ_1 the antibonding combinations involving the $6s$ atomic orbitals of the peripheral Au atoms, as well as the $6p_y$ orbital participation of the Au atom lying along the x axis. The second (β spin) component Ψ_2 shows the character of the spin-orbit mixing in the HOMO, and one can observe three-center bonding (involving $5d$ AO's) of the gold atom lying along the x axis and its nearest neighbors, while the other two atoms of the upper pentagon are in antibonding phases with respect to the three atoms below. Thus the E_F level of Au_{13} is characterized as having $6s$-$6s$ antibonding combinations and small bonding interactions involving $5d$ AO's that are introduced by spin-orbit coupling, due to the proximity of the $d_{5/2}$ band. It is clear from the orbital populations given in Table IV, from the orbital energy diagram given in Fig. 2, and the discussion given above, that relativistic effects in the icosahedral Au_{13} cluster are significant.

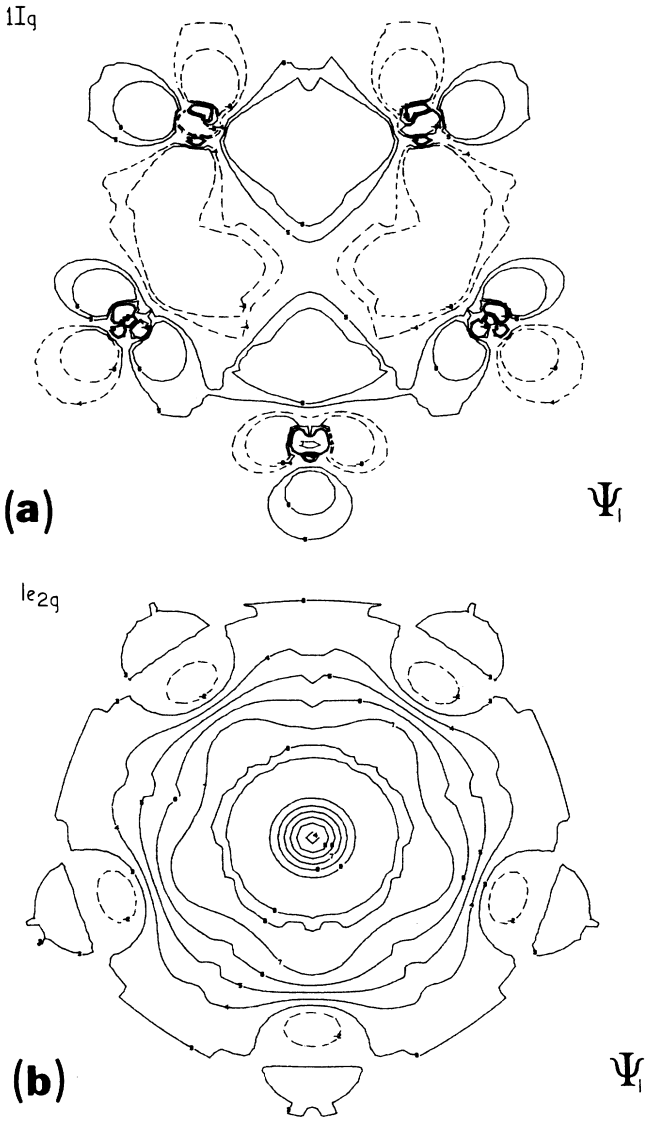

FIG. 4. (a) The dominant component of $1I_g$ passing ($z=2.33$ a.u.) through a pentagonal ring of atoms. (b) The dominant component of $1e_{2g}$ passing ($z=1.16$ a.u.) midway between the pentagon and the central atom.

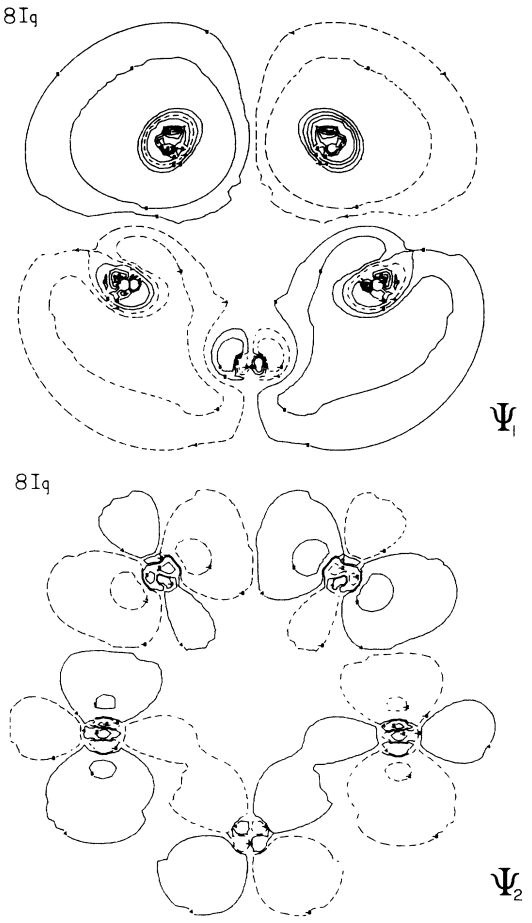

FIG. 5. The large components of the HOMO ($8I_g$) at $z=2.33$ a.u. The contour values of Ψ_1 and Ψ_2 are the same as in Fig. 3.

B. Band structure of icosahedral Au_{13} cluster

Although current relativistic band structure [such as RKKR and relativistic augmented plane wave (RAPW)] calculations are in good agreement with the x-ray photoemission spectroscopy (XPS) studies of crystalline gold[47] and ultraviolet photoemission spectroscopy (UPS) studies of clean surfaces of gold,[48] the situation is not so clear for heavy metallic clusters. In spite of recent accurate experimental data on the valence bands of gold clusters,[42–45] no detailed relativistic molecular-orbital calculations of neutral gold clusters have yet been reported. Since the DSW method is the molecular analog of the RKKR energy-band structure technique,[29] it is qualitatively interesting to compare the density-of-states (DOS) curves obtained experimentally[42–45] with the DOS (Gaussian-broadened discrete levels) calculated for the icosahedral Au_{13} cluster via a relativistic molecular-orbital (DSW) method. The DOS curves for the Au_{13} cluster, obtained from the nonrelativistic-limit and the relativistic (DSW) calculations are shown in Fig. 6 (with the broadening parameter equal to 0.35 eV) and important differences are noticeable. Figure 7 shows the valence-band spectra for different coverages of gold on carbon.[45] The spectra of the gold clusters on carbon substrate and the appropriately normalized spectra of the clean carbon were subtracted to yield spectra characteristic of the clusters themselves.[44,45] The nonrelativistic-DOS curve shows essentially five peaks of higher intensity than the DSW-DOS curve. The main characteristics of the nonrelativistic-DOS curve are that the two small peaks at higher energy (between the Fermi level E_F and -5 eV) correspond mainly to the occupied s band which just begins to overlap the main d band, while the low-energy peak corresponds mainly to the discrete nature of the central atom curves. The nonrelativistic Fermi level (E_F) is completely embedded in the s band and is quite well separated from the main d band. It is clear that the nonrelativistic-DOS curve differs significantly from those obtained experimentally,[42–45] as can be seen from Figs. 6 and 7.

The DSW-DOS curve shows essentially three main peaks, and it is evident that the s band overlaps almost completely the d band, and that the E_F level approaches closely the d band. The main two peaks are attributed to the spin-orbit coupling effect, and the drop in intensity of the DSW-DOS curve can be assigned to the enhanced s-d hybridization occurring in the valence band. The d-band width is 3.9 eV, and the d-band splitting of the Au_{13} cluster is 2.2 eV. These calculated values are in very good agreement with the experimental values obtained from the photoemission spectra of the valence band of gold clusters.[42–45] The calculated d-band width (for Au_{13}) is approximately 75% of the d-band width (5.24 eV) observed in crystalline gold,[47,49] and the d-band splitting is about 80% of the observed d-band splitting (2.8 eV) in the bulk

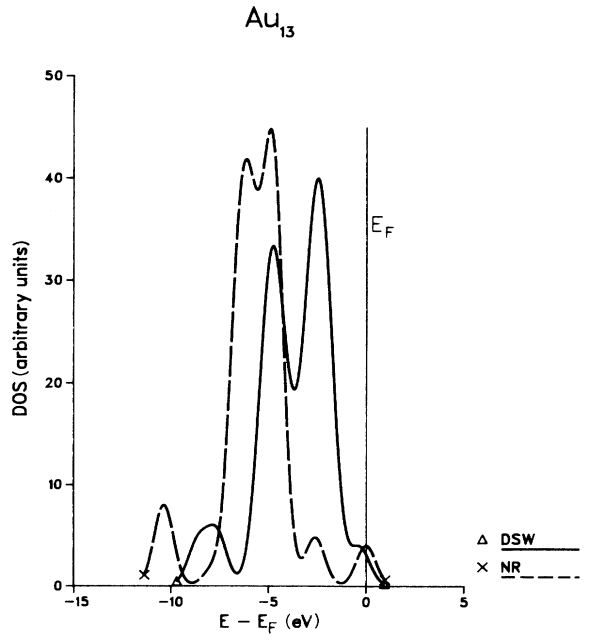

FIG. 6. Nonrelativistic (NR) limit and relativistic (DSW) Gaussian-broadened density of states (DOS). The energies are shifted in each case, so that the Fermi (E_F) level is at zero of energy.

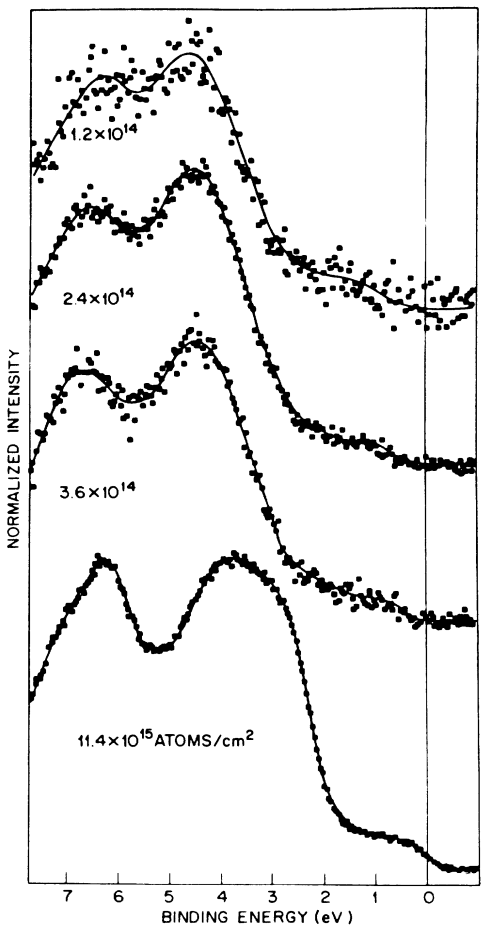

FIG. 7. Valence-band spectra of gold clusters on a vitreous carbon substrate. The substrate's contribution to each spectrum has been subtracted (Ref. 45).

metal.[43,47,49] The relativistic destabilization of the d band in Au_{13} is also evident from Fig. 6, since it is shifted to higher energies. It is clear from the above-mentioned results as well as from the DOS curves that relativity should be taken into account in elucidating the electronic structure of such heavy-atom clusters, and that nonrelativistic calculations give an unrealistic description of the density of states for such systems.

C. Transition state results

The use of the Slater's transition state (TS) method[50] is a convenient approach within local-density theory to estimate relaxation corrections (upon electron excitation) to ionization and excitation energies. In principle, the highest accuracy is obtained by performing TS calculations (until SCF convergence is reached) for every transition of interest. The predicted ionization potential and excitation energies are collected in Table V. The first ionization potential is predicted to be 8.45 eV, while the lowest allowed dipole electronic transition (involving the HOMO and the unoccupied $7I_u$ level) is predicted to occur at 1.74 eV. The other two transitions (arising from the top of the d band to the E_F level) are calculated to be at 1.70 and 2.03 eV. The latter transition could be assigned to the XPS transition from the d band to the E_F level observed at 2.04 eV in crystalline gold,[47] which is responsible for the characteristic color of solid gold.

TABLE V. Ionization potential and transition energies (eV).

Transition	DSW
$8I_g \rightarrow$ vacuum	8.45
$5q_u \rightarrow 8I_g$	1.70
$8I_g \rightarrow 7I_u$	1.74
$6I_u \rightarrow 8I_g$	2.03

IV. CONCLUSIONS

The calculations presented here represent the first detailed study of an icosahedral heavy metal cluster using the DSW method. The symmetry-adapted basis functions for the I_h^* (double) group are generated for the first time, and the resulting relativistic molecular orbitals are analyzed to discuss the relativistic effects in chemical bonding, which are manifested through significant s-d hybridization. It has been shown that the nonrelativistic calculation predicts a sextet as the ground state ^6A_g, whereas the fully relativistic treatment predicts the ground state to be a doublet ^2I_g. It has been found that the DOS curve obtained by the DSW calculation shows features similar to those observed for the DOS obtained from photoemission experiments on supported gold clusters, and that many more atoms (more than 13) are required to mimic the bulk metallic behavior. Since the knowledge of the electronic structure of metallic clusters is of pivotal importance in surface science, the approach (DSW) used here seems suitable for the elucidation of the electronic structure of large metallic clusters containing heavy atoms, in which relativistic effects are significant.

ACKNOWLEDGMENT

We are grateful to the Natural Sciences and Engineering Research Council (NSERC) of Canada for support through Grant No. A3598, as well as for a grant for the use of the Cray-1 computer at Dorval, Montreal.

*Current address: Department of Chemistry, University of Texas at Arlington, Box 19065, Arlington, Texas 76019.

[1]D. Schechtman, I. Blech, D. Gratias, and J. W. Cahn, Phys. Rev. Lett. **53**, 1951 (1984).
[2]P. A. Bancel, P. A. Heiney, P. W. Stephens, A. I. Goldman, and P. M. Horn, Phys. Rev. Lett. **54**, 2422 (1985).
[3]A. J. Melmed and R. Klein, Phys. Rev. Lett. **56**, 1478 (1986).
[4]D. M. Follstaedt and J. A. Knapp, Phys. Rev. Lett. **56**, 1827 (1986).
[5]W. A. Cassada, G. J. Shiflet, and S. J. Poon, Phys. Rev. Lett. **56**, 2276 (1986).
[6]K. Wade, *Electron Deficient Compounds* (Appleton-Century-Crofts, New York, 1971), pp. 56—58.
[7]H. C. Longuet-Higgins and M. de V. Roberts, Proc. R. Soc. London, Ser. A **230**, 110 (1955).
[8]S. Ogawa and S. Ino, J. Cryst. Growth **13**, 48 (1972).
[9]C. Solliard, Ph. Buffat, and F. Faes, J. Cryst. Growth **32**, 123 (1976).
[10]C. Y. Yang, K. Heinemann, M. J. Yacaman, and H. Poppa, Thin Solid Films **58**, 163 (1979).
[11]L. D. Marks and D. J. Smith, J. Cryst. Growth **54**, 425 (1981).
[12]L. B. Knight, R. W. Woodward, R. J. Van Zee, and W. Weltner, Jr., J. Chem. Phys. **79**, 5820 (1983).
[13]C. E. Briant, B. C. Theobald, J. W. White, L. K. Bell, and D. M. P. Mingos, J. Chem. Soc. Chem. Commun. 201 (1981).
[14]D. M. P. Mingos, J. Chem. Soc. Dalton Trans. 1163 (1976).
[15]D. R. Salahub, in *Contribution in Cluster Physics in Material Science and Technology,* edited by J. Davenas and P. Rabette (Nijhoff, The Hague, 1986), p. 104.
[16]M. E. Mc. Henry, M. E. Eberhart, R. C. O'Handley, and K. H. Johnson, Phys. Rev. Lett. **56**, 81 (1986).
[17]J. Demuynck, M. M. Rohmer, A. Strich, and A. Veillard, J. Chem. Phys. **75**, 3443 (1981).
[18]See, for example, Surf. Sci. **156** 3 (1985).
[19]M. D. Morse, M. E. Gensic, J. R. Health, and R. E. Smalley, J. Chem. Phys. **83**, 2293 (1985).
[20]J. Koutecky and P. Fantucci, Chem. Rev. **86**, 539 (1986).
[21]G. L. Malli and N. C. Pyper, Proc. R. Soc. London, Ser. A. **407**, 377 (1986).
[22]R. Arratia-Perez and G. L. Malli, Chem. Phys. Lett. **125**, 143 (1986).
[23]R. Arratia-Perez and G. L. Malli, J. Chem. Phys. **84**, 5891 (1986).
[24]K. H. Johnson, Adv. Quantum Chem. **7**, 143 (1973).
[25]C. Y. Yang and S. Rabii, Phys. Rev. A **12**, 362 (1975).
[26]C. Y. Yang, in *Relativistic Effects in Atoms, Molecules and*

Solids, edited by G. L. Malli (Plenum, New York, 1983), p. 335.
[27]C. Y. Yang and D. A. Case, in *Local Density Approximations in Quantum Chemistry and Solid State Physics,* edited by J. Dahl and J. P. Avery (Plenum, New York, 1984), p. 643.
[28]D. A. Case and C. Y. Yang, J. Chem. Phys. **72**, 3443 (1980).
[29]Y. Onodera and M. Okazaki, J. Phys. Soc. Jpn. **21**, 1273 (1966); S. Takada, Prog. Theor. Phys. **36**, 224 (1966).
[30]P. Pykko, Adv. Quantum Chem. **11**, 353 (1978).
[31]*Relativistic Effects in Atoms, Molecules, and Solids,* edited by G. L. Malli (Plenum, New York, 1983).
[32]R. Arratia-Perez and D. A. Case, Inorg. Chem. **23**, 3271 (1984).
[33]J. P. Lopez and D. A. Case, J. Chem. Phys. **81**, 4554 (1984).
[34]R. Arratia-Perez and C. Y. Yang, J. Chem. Phys. **83**, 4005 (1985).
[35]D. A. Case and J. P. Lopez, J. Chem. Phys. **80**, 3270 (1984).
[36]D. A. Case, J. Chem. Phys. **83**, 5792 (1985).
[37]C. Y. Yang, J. Chem. Phys. **68**, 2626 (1978).
[38]As defined in E. P. Wigner, *Group Theory* (Academic, New York, 1959).
[39]P. H. E. Meijer, Phys. Rev. **95**, 1443 (1954).
[40]J. Raynal, J. Math. Phys. **25**, 1187 (1984).
[41]This is an unpublished computer program written by C. Y. Yang based on Ref. 37.
[42]K. S. Liang, W. R. Salaneck, and I. A. Aksay, Solid State Commun. **19**, 329 (1976).
[43]H. Roulet, J. M. Mariot, G. Dufour, and C. F. Hague, J. Phys. F **10**, 1025 (1980).
[44]S. T. Lee, G. Apai, M. G. Mason, R. Benbow, and Z. Hurych, Phys. Rev. B **23**, 505 (1981).
[45]G. K. Wertheim, S. B. DiCenzo, and S. E. Younquist, Phys. Rev. Lett. **51**, 2310 (1983).
[46]C. E. Moore, *Atomic Energy Levels,* Natl. Bur. Stand. (U.S.) Circ. No. 474 (US GPO, Washington, DC, 1952), Vol. II.
[47]D. A. Shirley, Phys. Rev. B **5**, 4709 (1972).
[48]A. D. McLachlan, J. Liesegan, R. C. G. Leckey, and J. G. Jenkin, Phys. Rev. B **11**, 2877 (1975).
[49]It should be remarked that a more realistic comparison should be made between the photoemission DOS curves for crystalline gold and the corresponding calculated DOS for the cuboctahedral Au_{13} cluster because it is compatible with the metal fcc structure. Further work along these lines is in progress.
[50]J. C. Slater, *The Self-Consistent Field for Molecules and Solids* (McGraw-Hill, New York, 1974).